

# Geometrical optics: He-check setup

Matilde Dondi

July 20, 2024

## 1 He-check system concept

Various sources of uncertainties can arise in hadron therapy, impacting the treatment plan and necessitating an increase in the safety margin, thereby potentially reducing treatment benefits. Among these sources are anatomical changes, setup errors, and inaccuracies in proton stopping powers in different materials. To address these challenges, various dose verification systems have been developed. A real-time verification system that provides information on the ion beam range within the patient during treatment sessions is crucial to mitigate uncertainties. The He-Check system concept involves using  $^{12}\text{C}$  and  $^4\text{He}$  ions simultaneously, respectively for therapeutic treatment and verification purposes. This approach aims to avoid treatment interruptions for dose verification.

Carbon ions ( $^{+6}\text{C}$ ) and helium ions ( $^{+2}\text{He}$ ) can be accelerated together, due to the fact that they share the same magnetic rigidity ( $R = B\rho = pc/q$ ). This results in a mixed beam in which the two species have the same energy per nucleon. It is important to specify that while the rest mass-to-charge ratio of the carbon is 12/6 a.m.u., the ratio of He is 4.0026033/2 a.m.u. This slight difference in ratios results in a small difference in magnetic rigidity between the two ions, causing their orbits within the same magnetic field to have different radii. The accelerator's extraction mechanism utilizes a betatron core to push the beam stacks towards resonance. Due to their slightly different magnetic rigidities, helium particles reach resonance first and are consequently extracted first. Therefore, to utilize the mixed beam, it is necessary to discard the initial part of the extracted beam, which consists only of helium, and the final part, which consists only of carbon.

Carbon and helium ions have different ranges in matter due to their mass differences. At equal energy per nucleon and in the same medium, helium ions have a range approximately three times greater than carbon ions. The range of two particles with the same energy per nucleon in the same medium can be approximated as:

$$R_a(v) = \frac{m_a z_a^2}{m_b z_b^2} R_b(v). \quad (1)$$

In the case of carbon and helium, this formula yields a range ratio of 3:1 between helium and carbon.

Thanks to their nearly equal magnetic rigidity and differing ranges, it is feasible to simultaneously accelerate both beams. In this system, carbon deposits its dose to the tumor while helium passes through the patient and releases its energy in a detector. By measuring the residual range of helium exiting the patient and its position in coincidence, it is possible to reconstruct the density and thickness traversed, thus achieving real-time verification.

Figure 1 illustrates a schematic representation of the He-Check system.

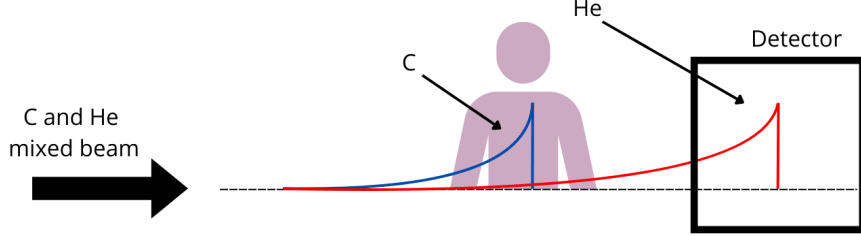


Figure 1: Schematic representation of the He-check idea.

The following sections provides a detailed explanation of the setup selected for the He-Check project as well as a study of the geometrical optics involved.

## 2 Setup

The setup consists of a  $20 \times 20 \text{ cm}$  ( $l_s$ ) plastic scintillator coupled with a scientific CMOS camera. The system is placed inside a box with walls completely black to minimize external light reaching the sensor. The box has a lateral aperture through which the particle beam can enter.

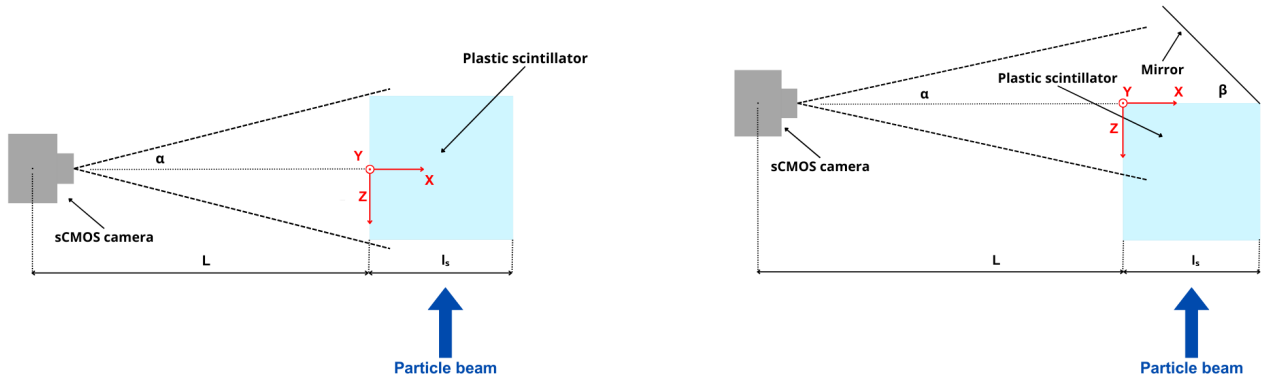


Figure 2: Schematic setup of the scintillator and camera seen from above in two main configurations: on the left, the camera is centered in the Y-Z directions of the scintillator; on the right, a mirror is added and the camera is aligned with the side of the scintillator and centered in the Y direction.

For a more accurate reconstruction of the light produced by the particle beam, an analytical study of the geometrical optics of the setup has been performed.

The centre of the coordinates used in this work is depicted in Figure 2, where the setup is viewed from above in the two different configurations. The origin of the Y coordinate, representing the height, is positioned at the middle of the scintillator. The camera is located at a distance  $L$  from the proximal side of the scintillator, centered in the Y direction as in Figure 2 and aligned with the origin of the coordinate system, but can be laterally moved along the Z direction. The particle beam is directed towards the Z direction, impacting the lateral side of the scintillator.

Two main configurations are shown in Figure 2: one with the camera centered in the middle of the scintillator in the Z direction, and the other with the camera aligned with the side of the scintillator. In the second configuration, a mirror is added as shown at an angle  $\beta$  relative to the side of the scintillator. The mirror enables observation of the X position of the light, facilitating reconstruction of the transverse position of the Bragg peak. In both figures,  $\alpha$  represents half of the camera's field of view angle along the Z direction.

The camera and scintillator specifications are detailed in Table 1 and Table 2, respectively.

Model	Andor Zyla 5.5 sCMOS
Sensor dimensions	$2560 \times 2160$ pixel, $16.6\text{ mm} \times 14\text{ mm}$
Pixel size	$6.5\text{ }\mu\text{m} \times 6.5\text{ }\mu\text{m}$
Full well capacity	$30000\text{ e}^-$
Dark current	$0.1\text{ e}^-/\text{pixel/s}$ at $0^\circ\text{C}$
A/D converter	Dual amplifier stage: 16-bit and 12-bit
Electrons per digital unit	$0.45\text{ e}^-/\text{ADU}$
Read-out noise	$2.5\text{ e}^-$ RMS
Cooling	Thermoelectrical
Producer and Model of the lens	Azure photonics 2520MX5M (to be checked)

Table 1: Camera characteristics

Model	BC-408 Plastic Scintillator
Dimensions	$20 \times 20 \times 20$
Light yield (% Antracene)	64
Emission wavelength (nm)	425
Main component decay constant (ns)	2.1
Attenuation length (cm)	380
Refraction index	1.58
Density ( $\text{g}/\text{cm}^2$ )	1.032
H:C ratio	1.101

Table 2: Scintillator characteristics

### 3 Lens parameters

The position of the camera relative to the scintillator is a crucial parameter to consider. From the distance  $L$ , it is possible to derive the Field Of View (FOV) of the camera in the Y and Z directions. Considering the sensor dimension  $h$  (in Table 1) and the focal length  $f$ , the field of view angle is given by:

$$\alpha = \arctan\left(\frac{h}{2f}\right) \quad (2)$$

From this equation the FOV can be calculated as:

$$FOV = \frac{Lh}{f} \quad (3)$$

Figure 3 illustrates a schematic representation of the field of view and its relation with the camera's sensor. Since the sensor is not perfectly square, the field of view differs slightly between the Y and Z directions. The camera is oriented such that the longer side of the sensor aligns with the Z direction. Figure 4 depicts the FOV of the camera for a fixed focal distance of 25 mm for the two different dimensions.

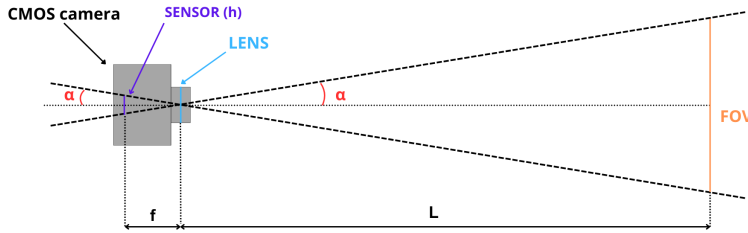


Figure 3: Schematic representation of the field of view.

When the camera is centered with respect to the scintillator, the frontal side of the scintillator can be seen completely in both dimensions already from 500 mm, while if the camera is moved laterally, the scintillator is not completely visible unless we reach 610 mm.

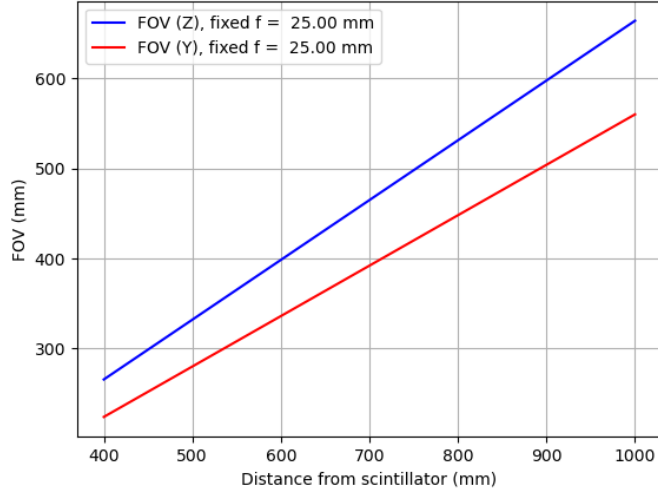


Figure 4: Field of view of the camera as a function of distance from the scintillator for both Z and Y directions.

Another important parameter to define is the depth of field, which is the distance between the nearest and farthest objects that are acceptably sharp in focus in an image. It is crucial that the entire scintillator remains in focus. The depth of field depends strongly on the focal distance  $f$ , the f-number  $F/$ , defined as the ratio of the focal length to the aperture diameter, and the circle of confusion. The circle of confusion is the diameter of the blurred image produced by a point-like object located outside the depth of field.

The distances from the camera of the nearest object in focus  $d_{prox}$  and farthest object in focus  $d_{dist}$  are given by:

$$d_{prox} = \frac{f^2 d}{f^2 - c(d-f)F/} \quad (4)$$

$$d_{dist} = \frac{f^2 d}{f^2 + c(d-f)F/} \quad (5)$$

where  $d$  is the focus distance.

The pixel dimension of the camera are  $6\text{ }\mu\text{m} \times 6\text{ }\mu\text{m}$ . Without any binning during the acquisition, the circle of confusion can be taken equal to the pixel dimension. Considering a focus length of the circle of confusion can be considered equal to the pixel dimension. Considering a focal length of 25 mm and an exposure time of 10 ms,  $F/16$  is the optimal aperture to obtain a clear image. At a focus distance of 70 cm, the depth of field covers the entire dimension of the scintillator, ensuring it appears completely in focus.

## 4 Estimate of the lens position

The camera lens used in the setup consists of a system of multiple lenses. Hence, it is necessary to estimate a virtual position of a lens that would correspond to this system. Given the focal distance of the lens is 25 mm, we can assume at this distance the virtual position of the camera sensor. The length  $L$ , introduced earlier in section 2, represents the distance from the scintillator to the position of this virtual lens. To determine the position of the virtual lens, field of view measurements were conducted at various distances from the camera's support. These measurements were subjected to a linear fit, and the intersection point of the straight line with the X-axis indicates the position of the virtual lens. The results of these measurements are shown in Figure 5.

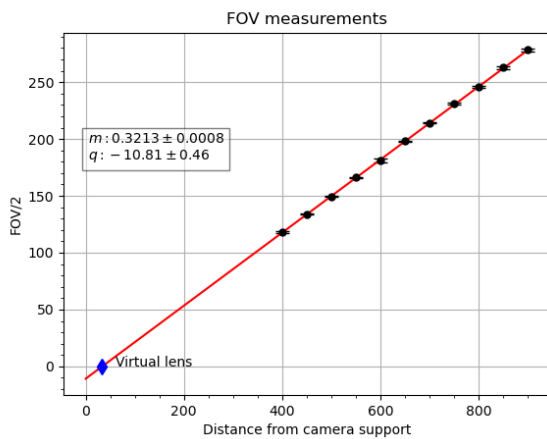


Figure 5: Field of view measurements at different distances from the camera support with the performed linear fit. The estimated position of the virtual lens is also shown.

The virtual lens is positioned at  $(34 \pm 2)$  mm from the camera's support. It is important to note that the FOV value depends on the camera's focusing settings and the positioning of the camera's objective. In reality, the camera lens comprises a complex system of lenses rather than a single lens. Therefore, this measurement serves as an estimate rather than an exact value.

## 5 Refraction

The scintillator has a refractive index of  $n_2 = 1.58$ , which differs from the refractive index of air,  $n_1 = 1$ . Correctly reconstructing the position of an object inside the scintillator requires consideration of the refraction of optical rays entering from outside. In Figure 6 is illustrated the situation of an optical ray coming from behind the scintillator.

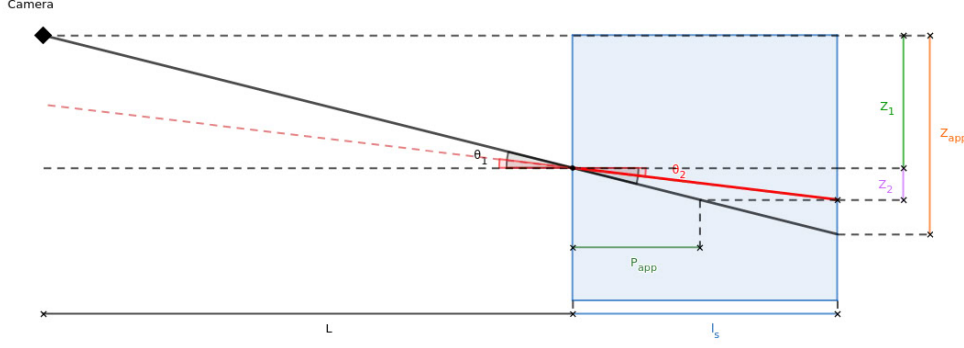


Figure 6: Schematic representation of the refraction of an optical ray coming from an object positioned behind the scintillator.

From the picture, the real position of the object  $Z_{true}$  and the  $Z_{apparent}$  are given by:

$$Z_{true} = Z_1 + Z_2 = L \tan \theta_1 + l_s \tan \theta_2 \quad (6)$$

$$Z_{app} = (L + l_s) \tan \theta_1 \quad (7)$$

where  $\theta_1$  and  $\theta_2$  are the incident angles of the optical ray in air and inside the scintillator, respectively.

The two angles are related by the Snell's law:  $n_1 \sin \theta_1 = n_2 \sin \theta_2$ . The Z positions are calculated with respect to the reference frame introduced in section 2. An object positioned behind the scintillator will appear in the camera at an apparent position at a distance  $L + P_{app}$  from the camera, where  $P_{app} = Z_2 / \tan \theta_1$ . This calculation applies similarly in the Y direction. If the optical ray originates not from directly behind the scintillator but from a distance  $X_{true}$  from the farthest side of the scintillator to the camera, the formulas adjust accordingly to  $Z_{app} = (L + l_s - X_{true})$ .

When the scintillator is positioned at 650 mm from the camera, the refraction of light results in a maximum magnification effect of approximately  $\sim 10\%$ . This effect was verified by placing a sheet of graph paper behind the scintillator and measuring the position of a dot through the scintillator relative to its known position on the graph paper.

## 6 Reflection

Another significant effect that occurs within the scintillator is reflection. Optical rays are internally reflected from the lateral sides of the scintillator, and through analytical analysis, it is possible to calculate the actual position of an object after single internal reflection. For simplicity, let's start with an optical ray originating from behind the scintillator and then proceed with the calculations inside.

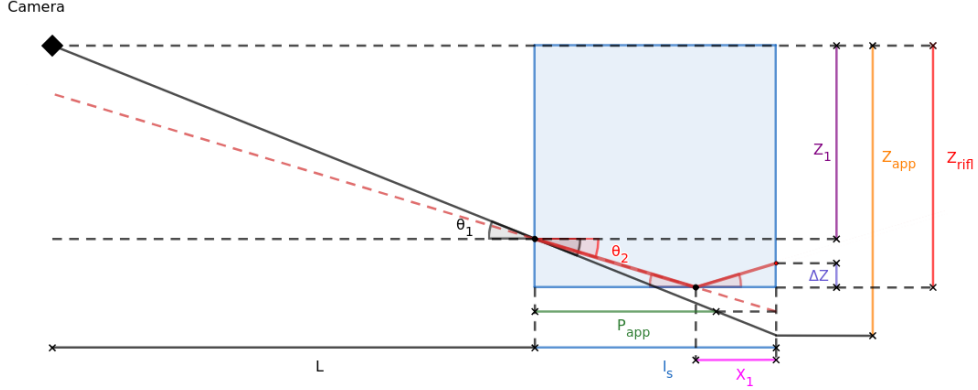


Figure 7: Schematic view of the reflection of an optical ray originating from behind the scintillator.

From Figure 7, which illustrates a schematic view of reflection, the apparent ZZ position of an object behind the scintillator is still given by Equation 7. As previously mentioned in Equation 6,  $Z_1 = L \tan(\theta_1)$ . The true position can be derived through the following calculations:

$$x_1 = (Z_{refl} - Z_1) \frac{1}{\tan \theta_2} \quad (8)$$

$$\Delta z = (l_s - x_1) \tan \theta_2 \quad (9)$$

$$Z_{true} = Z_{refl} - \Delta z \quad (10)$$

where  $Z_{refl}$  indicates the position of the scintillator side where reflection occurs relative to the camera. An object positioned behind the scintillator will appear in the camera as if it were located at a distance  $L + P_{app}$  from the camera, where  $P_{app} = (Z_{refl} + \Delta z - Z_1) / \tan(\theta_1)$ . To observe reflection, the values of variables  $x_1$  and  $\Delta z$  must be positive: objects in positions that do not meet this requirement are not reflected or their reflection does not reach the camera. For instance, with the camera positioned as in Figure 7, at a distance  $L = 650$  mm, only the last 37.9 mm in the Z direction are reflected, perceived by the camera as 41.6 mm due to refraction. Light originating from behind the scintillator is the most affected by reflection. In the formulas above, to determine the true position of an optical ray originating from a distance X from the proximal side of the camera, replace  $l_s$  with X, noting that fewer positions are visible through reflection. The same calculations apply for the Y dimension, considering refraction.

## 7 Mirror setup

As mentioned in section 2, in the configuration where the camera is aligned with the side of the scintillator, a mirror can be added to capture an image of the lateral position of the light

emitted by a particle beam. This setup is depicted in Figure 2 on the right, with the mirror positioned at an angle of  $\beta$  relative to the side of the scintillator.

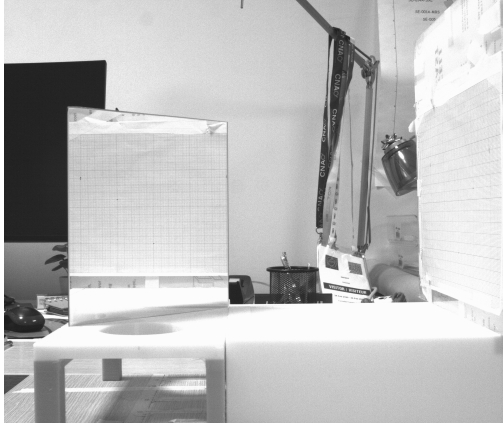


Figure 8: The mirror is positioned at a  $45^\circ$  angle relative to the camera’s line of sight, with the system placed at a distance of 650 cm. A sheet of graph paper is positioned at a minimum distance of 220 cm, which corresponds to the lateral side of the scintillator. From this image, it is evident that at a  $45^\circ$  angle, the graph paper is reflected straight while maintaining the original distances.

In reality, the setup differs slightly because the scintillator is positioned on a support that leaves a margin of 2.2 cm. Consequently, the edge of the mirror does not touch the scintillator but instead maintains a distance of 2.2 cm from it. The mirror itself is a square of the same dimensions as the scintillator,  $l_s = 200$  mm. The simplest and effective configuration chosen is  $\beta = 45^\circ$ , where the lateral side of the scintillator is reflected straight, as illustrated in Figure 8, due to the perpendicular reflection of optical rays. The reflection of the closer side (AB in Figure 9) of the scintillator, as seen from the camera, is at a distance equal to the distance of side BD from the camera plus 2 cm, laying on the plane  $P$  represented. Due to the dimension of the mirror and the angle chosen, AB is not reflected entirely.

In Figure 9, a schematic view of the setup and the calculation procedure for determining the reflected portion of the scintillator’s lateral side is presented. Propagating an optical ray from the last visible point of the scintillator to the edge of the mirror, it reflects with the same incident angle and reaches the camera. It can be demonstrated that the angle formed by this optical ray (shown in red in Figure 9) equals the angle  $\alpha$  depicted.

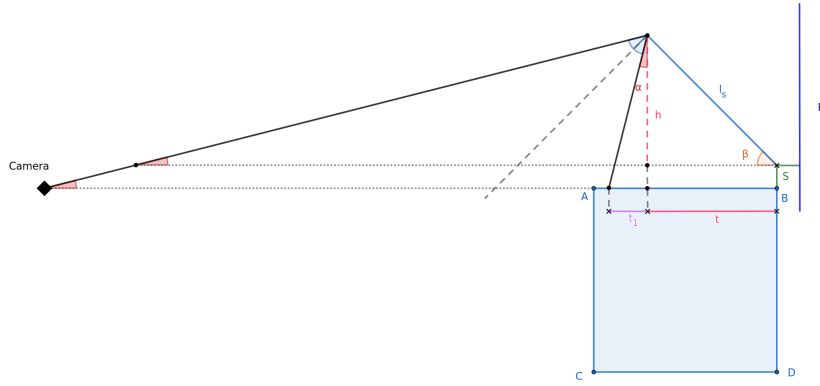


Figure 9: Schematic view of the mirror setup with a visual representation of the calculation used to determine the reflected portion of the lateral side of the scintillator.

Given the variables in Figure 9, the following equations hold:

$$h = t = l_s \sin \beta \quad (11)$$

$$t_1 = (h + s) \tan \alpha \quad (12)$$

$$\tan \alpha = \frac{h + S}{L + l_s - t} \quad (13)$$

where  $L$  is the usual distance between the camera and the closest side of the scintillator AC,  $l_s$  denotes the dimension of both the scintillator and the mirror, and  $S$  is the 2 cm distance between the mirror and the scintillator. The visible part of AB in the mirror thus amounts to  $t + t_1$ . For instance, at a distance  $L = 650$  mm, only approximately 179 mm are visible. Similarly, the other edge of the same face of the scintillator, B, is not fully contained within the mirror, as the mirror is positioned 2 cm away from the scintillator. In this case, the portion of the face not reflected in the mirror is sufficiently small to be considered negligible. To reflect the entire scintillator, a larger mirror could be chosen, or alternatively, the mirror could be positioned at an angle greater than  $45^\circ$ . However, in the latter case, the reflected image would not precisely match the original. The reflected image would appear behind the mirror at an angle  $\beta$  relative to the scintillator. Reconstructing this image would be more complex because each point of the reflected image is at a different depth relative to the camera, thus having a different value in mm/pixels. Hence, the optimal solution would be to opt for a larger mirror to encompass the entire scintillator; a dimension of 230 cm would suffice.

Regarding the further side of the scintillator relative to the mirror, CD, edge C is reflected, while D is not visible in the mirror reflection. Specifically, from D, almost half a centimeter is missing from the reflection in the mirror. To resolve this issue, two solutions are possible: eliminate the 2 cm gap between the mirror and the scintillator, or move the mirror the same distance behind the scintillator. With the second option, a larger mirror, such as one

measuring 240 mm, would be necessary to see point A adequately.

The information from the mirror can provide the X position of a point inside the scintillator. To correctly reconstruct the X position, it is necessary to consider the refraction of light. As previously done, the easiest approach is to start with a point positioned at the back of the scintillator, which corresponds to  $Z = l_s$ . The geometric construction of the system is represented in Figure 10.

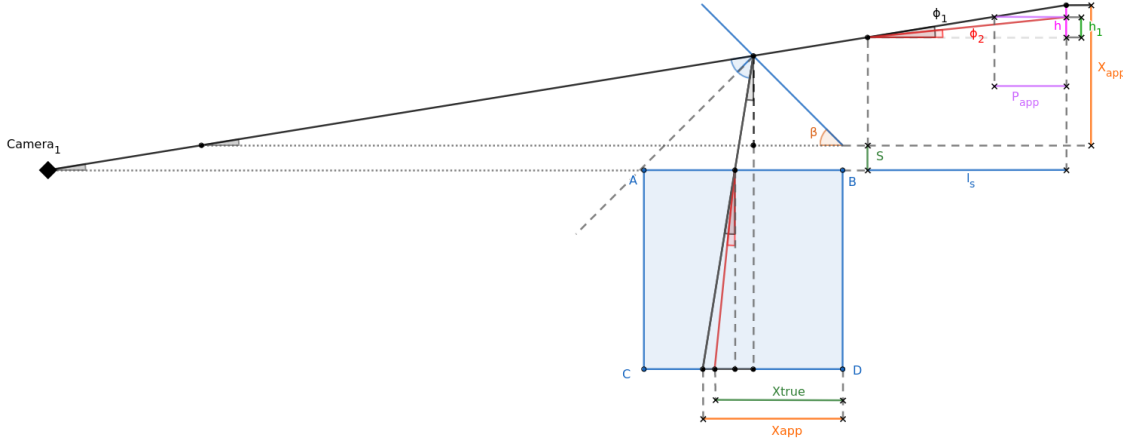


Figure 10: Geometric construction used to calculate the X position of a point located at  $Z = l_s$  considering refraction inside the scintillator.

Considering the variables introduced in the figure, the following equations are valid:

$$\tan \phi_1 = \frac{X_{app} + s}{L + 2l_s + s} \quad (14)$$

$$X_{true} = X_{app} - (h - h_1) = X_{app} - l_s(\tan \phi_1 - \tan \phi_2) \quad (15)$$

where the two angles are related by the Snell's law. The object will appear at an apparent position  $P_{app}$  behind the mirror, as shown in Figure 10.

The X position of the point relative to the side of the scintillator closest to the camera is  $X'_{true} = l_s - X_{true}$ .

If instead the object is not at  $Z = l_s$ , but at certain  $Z_{true}$ , the calculations changes as follows:

$$\tan \phi_1 = \frac{X_{app} + s}{L + l_s + Z_{true} + s} \quad (16)$$

$$X_{true} = X_{app} - (h - h_1) = X_{app} - Z_{true}(\tan \phi_1 - \tan \phi_2) \quad (17)$$

while the other equations remain the same.

## 8 Position reconstruction

The reconstruction of the position of a certain point inside the scintillator requires information about all three coordinates, with the X coordinate given by the mirror. The apparent positions due to refraction can be estimated given the number of pixels for that position,  $n_{pixels}$  and the mm/pixel corresponding to that specific depth with respect to the camera. Calling  $K_d$  the mm/pixel corresponding to a depth  $d$  from the proximal side of the scintillator to the camera, which is at  $d = 0$ , it is possible to obtain:

$$K_d = d \left( \frac{K_s - K_0}{l_s} + K_0 \right) \quad (18)$$

where  $K_s$  is the value of the mm/pixel at a distance  $l_s$ , which in this setup is equal to 200 mm. Using this equation the apparent position in X, Y and Z will be given by:

$$X_{app} = d \left( \frac{K_s - K_0}{l_s} + K_0 \right) n_{xpixels} = (l_s + s + Z_{true}) \left( \frac{K_s - K_0}{l_s} + K_0 \right) n_{xpixels} \quad (19)$$

$$Y_{app} = d \left( \frac{K_s - K_0}{l_s} + K_0 \right) n_{ypixels} = (l_s - X_{true}) \left( \frac{K_s - K_0}{l_s} + K_0 \right) n_{ypixels} \quad (20)$$

$$Z_{app} = d \left( \frac{K_s - K_0}{l_s} + K_0 \right) n_{zpixels} = (l_s - X_{true}) \left( \frac{K_s - K_0}{l_s} + K_0 \right) n_{zpixels} \quad (21)$$

The variables  $n_{xpixels}$ ,  $n_{ypixels}$  and  $n_{zpixels}$  are the number of pixels visible in the image produced by the camera corresponding to the apparent positions of a certain point that needs to be reconstructed. Combining Equation 6 and Equation 7, it is possible to obtain:

$$Z_{true} = \frac{L Z_{app}}{L + l_s - X_{true}} + (l_s - X_{true}) \tan \left( \arcsin \left( \frac{\sin(Z_{app}/(L + l_s))}{n_2} \right) \right) \quad (22)$$

and for the Y position it is valid:

$$Y_{true} = \frac{L Y_{app}}{L + l_s - X_{true}} + (l_s - X_{true}) \tan \left( \arcsin \left( \frac{\sin(Y_{app}/(L + l_s))}{n_2} \right) \right) \quad (23)$$

The  $X'_{true}$  position from the side of the scintillator closer to the camera, as already mentioned in section 7, is:

$$X'_{true} = l_s - X_{true} = l_s - X_{app} - Z_{true} (\tan \phi_1 - \tan \left( \arcsin \left( \frac{\sin \phi_1}{n_2} \right) \right)) \quad (24)$$

with  $X_{true}$  shown in Figure 10 and  $\tan \phi_1$  given by Equation 16.

## 9 Image acquisition and analysis

### 9.1 Acquisition setup and parameters

A preliminary image acquisition with the particle beam has been carried out to test the calculations and formulas derived so far. The setup used was the one shown in Figure 2 on the right, with the camera aligned laterally with the scintillator and the beam coming from the Z direction.

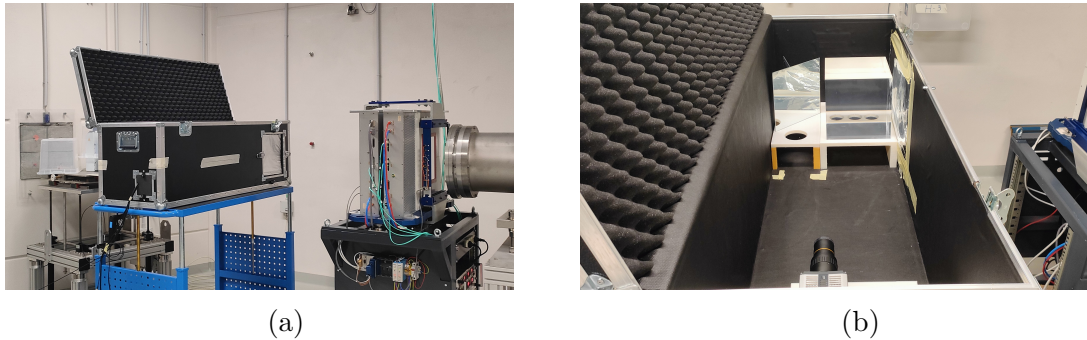


Figure 11: Setup inside the experimental room at CNAO: Figure 11a shows the box containing the setup with the lateral window in front of the particle beam; the aperture for the particles is also visible. Figure 11b shows the scintillator and the mirror correctly positioned inside the box.

The measurements were taken at a distance of  $L = 650$  mm from the camera to capture a complete view of both the scintillator and the mirror. After aligning the setup and positioning the box correctly, a reference image with the lights on was taken. From this image, the values of  $K_0$  and  $K_s$  mentioned in Equation 18 were obtained by measuring the number of pixels of objects at a specific distance with a known length. The value of  $K_0$  was determined knowing that the scintillator side closer to the camera is positioned at  $d = 0$  and its length is 200 mm, giving  $K_0 = 0.16$ .  $K_s$  was obtained from the mirror side positioned at  $d = 200$  mm, which is also 200 mm long, resulting in  $K_s = 0.21$ .

Some background images were also taken to serve as a baseline reference and to be subtracted from the subsequent images acquired. All the images taken are encoded as uint16 (unsigned integer), so the pixel intensity can range from 0 to 65535. When performing the subtraction, it is important to handle the images correctly by transforming the unsigned integers into signed integers since some pixels resulting from the subtraction can be negative. In such cases, the pixel value is set to 0.

The background images were taken with the box closed under different lighting conditions: with the lights on, off, and with and without a dark blanket above. All these images exhibited a mean pixel intensity value of around 110, without significant differences among them, indicating that the box is already quite effective at blocking any external light sources.

All the images were acquired with the camera set to External Trigger, using the first start-of-spill signal as the trigger signal. The camera acquired a kinetic series of images whose

length was set manually. The images were taken by irradiating the scintillator with proton beams at different energies corresponding to depths in water of 30 mm, 60 mm and 101 mm. The proton beam was delivered in a grid of 9 spots separated by 30 mm, each containing  $10 \times 10^6$  particles. The chosen exposure time for the acquisition was 50 ms and the diaphragm aperture was set at F/16.

## 9.2 Image analysis

This section presents the analysis of the images obtained with the proton beam.

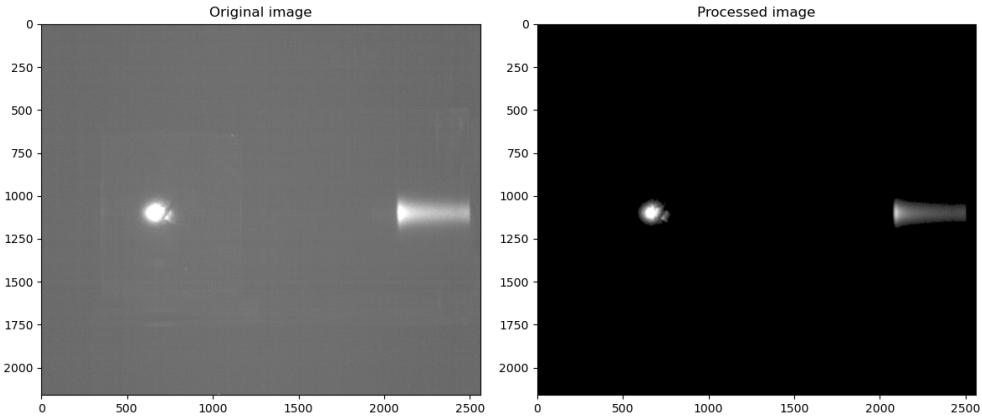


Figure 12: Image obtained from the camera and the corresponding one with background subtraction. The images have been rescaled with intensities from 0 to 255 to better visualize the light produced by the particle beam. In this case, it was a beam of protons with a 60 mm range in water, corresponding to an energy of 90 MeV.

Figure 12 shows an image obtained from the camera and the corresponding image obtained by subtracting the background. On the right side of the image, the range of the particles in the scintillator is visible, while on the left, there is the spot corresponding to the reflection in the mirror. A median filter was also applied to the images to remove noise spots caused by hot pixels. To reconstruct the range correctly, a Python code was developed. The goal is to reconstruct, using the equations summarized in section 8, the position of a luminous point located at the Bragg peak. In Figure 13 are shown the intensities of the image in Figure 12 integrated along the Y axis. On the right side, the characteristic shape of the Bragg peak is clearly visible. The last 197 pixels of the peak before the intensity drop (corresponding to the region outside the scintillator) are due to the reflection of light inside the scintillator.

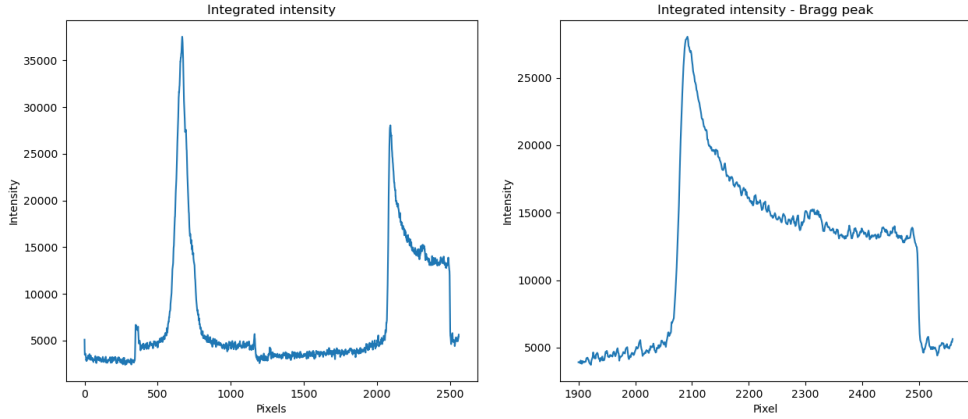


Figure 13: Integrated intensities along the vertical direction of the image. On the left, the total image is shown, where the peaks related to the spot in the mirror and the Bragg peak are visible. On the right, a zoom of the Bragg peak is shown. The plot refers to the image in Figure 12, protons at 90 MeV.

Firstly, from the image the code obtains the pixels corresponding to the Bragg peak and the center of the spot in the mirror, with two different methods.

- Integration method: the code integrates the luminosity along the y-axis to obtain the range of the particle and x positions from the 1D plot in Figure 13. Then it integrates the luminosity along the x-axis to obtain the y position.
- Clusterization method: it finds the two clusters corresponding to the track in the scintillator and spot in the mirror. In the cluster corresponding to the mirror spot it finds the center and from the other cluster the Bragg peak position.

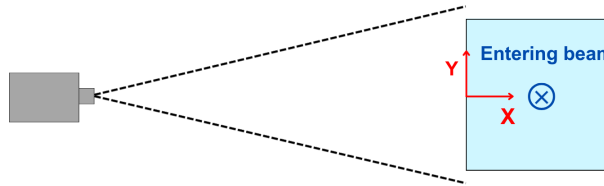


Figure 14: Schematic view of the setup seen from the direction of the beam entering the foil. The coordinate system used in the following results is also shown from this perspective.

These pixel positions are then used to evaluate  $n_{xpixel}$  and  $n_{zpixel}$  introduced in Equation 19 and Equation 21.

The system of equation presented in section 8 is then solved numerically, yielding the values of  $Z_{true}$  from the center of the image, where the camera is aligned, and  $X'_{true}$  from the side of the scintillator closer to the camera. The value of the range is then simply obtained by subtracting

$Z_{true}$  from  $l_s$ , the length of the scintillator. To help visualize the X and Y positions, Figure 14 provides a schematic representation of the setup seen laterally from the direction of the beam.

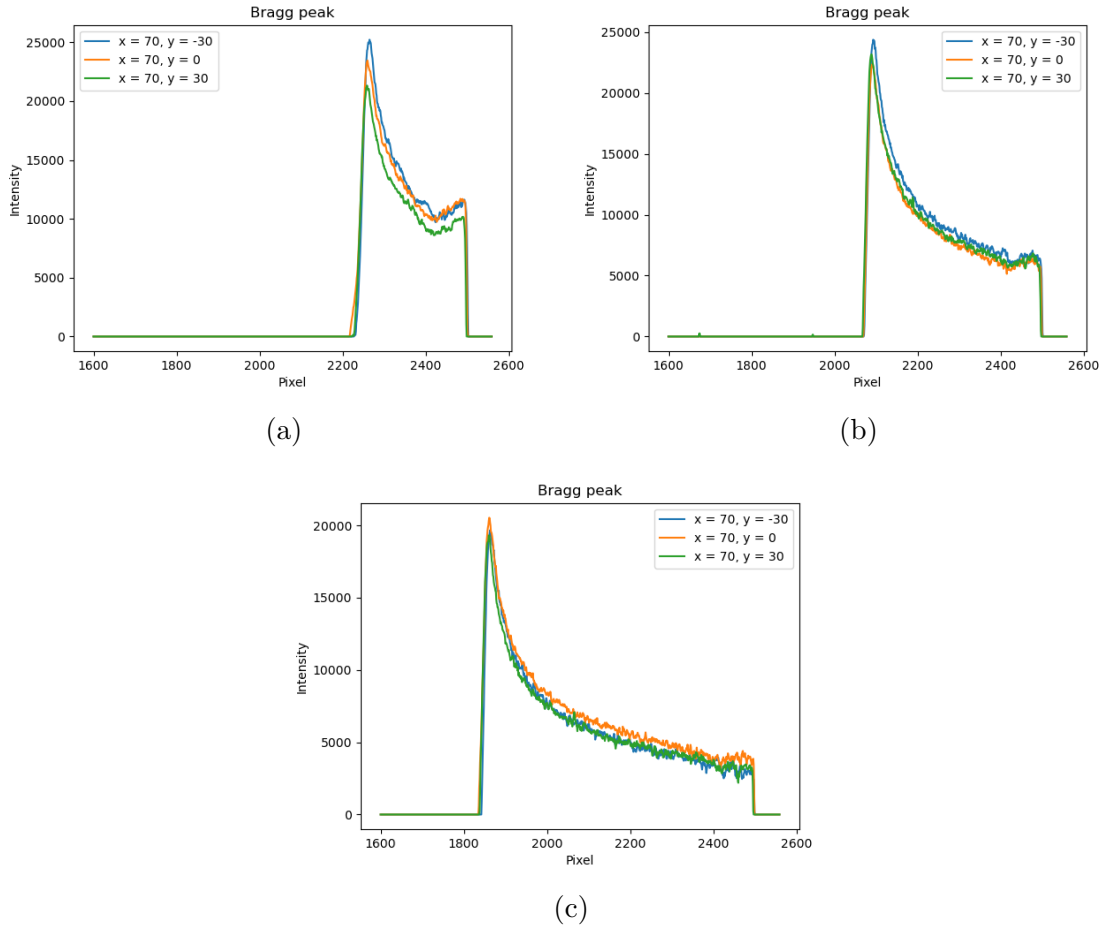


Figure 15: Luminous signal integrated in y coming from the scintillator. The characteristic shape of the Bragg peak is clearly visible. From the top, protons with a range in water of 30 mm, 60 mm, and 101 mm. For each image, the range is shown at different y positions of the beam but at the same depth. From the plot corresponding to 30 mm range, it is also possible to spot a region in which the curve changes shape, starting from around pixel 2300, corresponding to the reflection inside the scintillator.

Figure 15 shows the ranges at different X positions for protons at 90 MeV. As expected, at the same depth, the ranges have the same pixel length.

<b>X<sub>ref</sub></b>	<b>Y<sub>ref</sub></b>	<b>X</b>	<b>Y</b>	<b>Range</b>	<b>X<sub>clust</sub></b>	<b>Y<sub>clust</sub></b>	<b>Range<sub>clust</sub></b>
130	-30	140.3	-32.5	32.2	143.4	-34.0	31.6
100	-30	110.7	-32.5	32.1	110.9	-33.7	31.9
70	-30	81.6	-31.9	31.7	82.6	-31.7	31.6
70	0	81.6	-2.4	32.2	85.0	-3.8	31.6
100	0	111.7	-2.7	32.5	114.1	-3.9	32.0
130	0	140.3	-2.2	32.8	141.9	-2.4	32.1
130	30	141.5	27.4	32.8	138.6	25.7	33.0
100	30	111.4	26.9	32.5	109.3	26.1	32.8
70	30	81.9	27.4	32.5	82.8	26.2	32.2

Table 3: Results of image analysis for protons at 62 MeV with a range in water of 30 mm. ( $X_{\text{ref}}$ ,  $Y_{\text{ref}}$ ) are the reference beam position, ( $X$ ,  $Y$ ) are the actual beam positions, Range is the range calculated with the integration method, ( $X_{\text{clust}}$ ,  $Y_{\text{clust}}$ ) are the actual beam positions calculated with the clusterization method and  $\text{Range}_{\text{clust}}$  is the range calculated with the clusterization method.

<b>X<sub>ref</sub></b>	<b>Y<sub>ref</sub></b>	<b>X</b>	<b>Y</b>	<b>X<sub>clust</sub></b>	<b>Y<sub>clust</sub></b>	<b>Range</b>	<b>Range<sub>clust</sub></b>
130	-30	138.6	-33.0	61.6	140.9	-34.1	61.3
100	-30	110.5	-33.4	61.4	115.4	-34.1	60.6
70	-30	82.4	-33.3	60.9	84.7	-34.0	60.4
70	0	80.6	-2.8	61.4	82.6	-3.8	61.0
100	0	111.2	-3.5	61.7	112.9	-4.1	61.3
130	0	138.8	-3.6	61.9	140.7	-4.2	61.7
130	30	141.2	26.5	62.0	142.6	25.8	61.8
100	30	111.7	26.9	62.0	111.7	26.3	61.4
70	30	81.5	27.2	61.5	83.6	26.1	61.2

Table 4: Results of image analysis for protons at 90 MeV with a range in water of 60 mm. ( $X_{\text{ref}}$ ,  $Y_{\text{ref}}$ ) are the reference beam position, ( $X$ ,  $Y$ ) are the actual beam positions, Range is the range calculated with the integration method, ( $X_{\text{clust}}$ ,  $Y_{\text{clust}}$ ) are the actual beam positions calculated with the clusterization method and  $\text{Range}_{\text{clust}}$  is the range calculated with the clusterization method.

<b>X<sub>ref</sub></b>	<b>Y<sub>ref</sub></b>	<b>X</b>	<b>Y</b>	<b>Range</b>	<b>X<sub>clust</sub></b>	<b>Y<sub>clust</sub></b>	<b>Range<sub>clust</sub></b>
130	-30	138.6	-33.0	101.3	137.3	-33.1	101.1
100	-30	110.5	-33.4	101.0	109.7	-33.0	100.7
70	-30	82.4	-33.3	100.4	83.5	-33.0	100.1
70	0	80.8	-2.8	101.1	86.5	-4.0	100.5
100	0	111.4	-3.5	101.4	118.4	-4.1	100.6
130	0	137.8	-2.9	101.6	141.9	-4.2	101.0
130	30	139.2	27.5	101.8	138.7	26.1	101.7
100	30	111.8	27.6	101.5	111.8	26.3	101.3
70	30	81.7	27.6	101.2	84.7	26.4	100.8

Table 5: Results of image analysis for protons at 118 MeV with a range in water of 101 mm. ( $X_{\text{ref}}$ ,  $Y_{\text{ref}}$ ) are the reference beam position, ( $X$ ,  $Y$ ) are the actual beam positions, Range is the range calculated with the integration method, ( $X_{\text{clust}}$ ,  $Y_{\text{clust}}$ ) are the actual beam positions calculated with the clusterization method and  $\text{Range}_{\text{clust}}$  is the range calculated with the clusterization method.

The results obtained with the two methods for protons with ranges of 30 mm, 60 mm and 101 mm, corresponding to 62 MeV, 90 MeV and 118 MeV are shown respectively in Table 3, Table 4 and Table 5. In the first two columns of the tables, the reference positions in X and Y of the spots assuming perfect alignment of the setup with the beam are given. The values of the Y coordinate exhibit slight variations from their reference values and are all compatible, indicating a setup misalignment along Y of approximately 3 mm. However, the X values show clear discrepancies compared to their references and also differ among themselves. These discrepancies may be due to a misalignment of the setup in the X coordinate, amounting to nearly 1 cm. In addition some spots in the mirror lack clear definition, making it challenging to accurately identify the central pixel.

The range values obtained from the analysis appear to be quite compatible among themselves within 1 mm with both methods. Considering that inside the scintillator, the proton ranges in the three cases are equal to 31 mm, 61 mm and 101 mm, the values calculated are compatible with the expected ones.